Inorganic Chemistry

Article

pubs.acs.org/IC

Revelation of the Photoactive Species in the Photocatalytic Dimerization of α-Methylstyrene by a Dinuclear Ruthenium–Palladium Complex

Kei Murata,[†,‡] Akiko Inagaki,[†,§,∥] Munetaka Akita,[†] Jean-François Halet,*[,‡] and Karine Costuas*[,‡]

[†]Chemical Resources Laboratory, Tokyo Institute of Technology, R1-27, 4259 Nagatsuta, Midori-ku, Yokohama 226-8503, Japan

[‡]Institut des Sciences Chimiques de Rennes, UMR 6226 CNRS - Université de Rennes 1, F-35042, Rennes cedex, France

[§]Department of Chemistry, Faculty of Science and Engineering, Tokyo Metropolitan University, 1-1 minami Osawa, Hachioji, Tokyo 192-0397, Japan

Supporting Information

ABSTRACT: A quantum chemical study of the photocatalytic dimerization of α-methylstyrene catalyzed by a dinuclear ruthenium–palladium complex was performed at the DFT/TD-DFT level in order to find the key steps of the catalytic reaction. This study reveals that the second insertion of α-methylstyrene is the rate-determining step and that it proceeds via triplet excited states of an intermediate complex. These excited states have geometries significantly different from that of the reactant, especially within the coordination sphere of the Pd unit. Indeed, one Pd–carbon bond is considerably lengthened, favoring the insertion process. These results open up the possibilities to optimize the process by fine modulation of the catalyst structure.

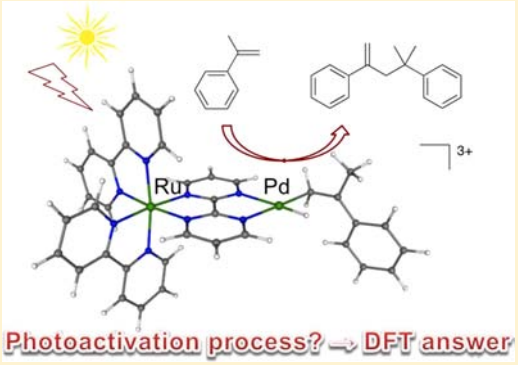

INTRODUCTION

Utilization of huge and inexhaustible solar energy in chemical reactions has attracted much attention because of recent important issues, such as global warming, environmental pollution, and energy resource depletion caused by high dependency on fossil fuels. Mimicking photosynthesis, coordination chemists have developed over the last decades complexes aiming at achieving photosyntheses with visible light.[1] In this area, ruthenium–polypyridyl complexes are widely used as photosensitizers because of their outstanding properties, such as visible light absorption, high luminescent quantum yields, and long excited-state lifetimes.[2] In another domain, photocatalytic hydrogen production from water and CO_2 reduction were also recently achieved with this kind of complex.[3] Combinations of a photosensitizer and a reactive center can provide interesting new catalysts.[2c,4] Several bimetallic catalysts containing the ruthenium–polypyridyl moiety linked to a transition-metal center, such as platinum[5] or rhenium–carbonyl[4,6] species, have been reported. However, the number of reported reactions is still limited, in particular for organic syntheses.

Following this reasoning, some of us reported the synthesis of the complex $[Ru(bpy)_2(bpm)PdMe(OCMe_2)](BF_4)_3$ (**1**) (bpy = 2,2′-bipyridyl, bpm = 2,2′-bipyrimidine) that combines an 18-electron ruthenium–polypyridyl moiety and a 16-electron palladium–alkyl unit bridged by a 2,2′-bipyrimidine ligand (see Chart 1).[7]

Chart 1

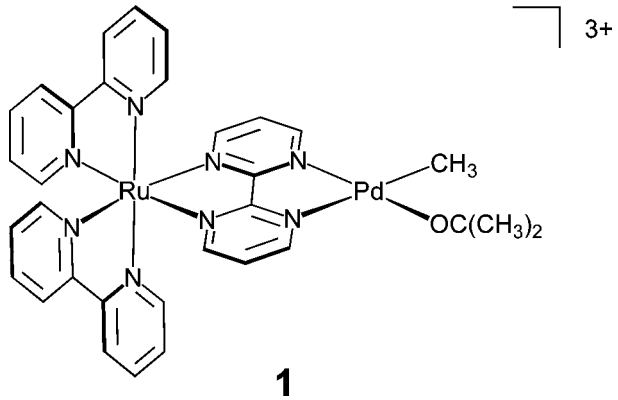

1

Compound **1** was shown to induce catalytic dimerization of α-methylstyrene (AMS) upon visible light irradiation (Scheme 1). It was originally proposed that visible light is absorbed by the ruthenium part of the molecule and that the relaxation of its excited state leads to the catalytic activation of the palladium center. Indeed, control experiments revealed that the ruthenium unit and the palladium center should be connected in a dinuclear structure to induce catalysis activity. In a recent paper, we have demonstrated that substituting the bipyridine

Received: March 18, 2013
Published: June 21, 2013

   dx.doi.org/10.1021/ic400666v | Inorg. Chem. 2013, 52, 8030–8039

Scheme 1. Photocatalytic Dimerization of α-Methylstyrene (AMS) by 1

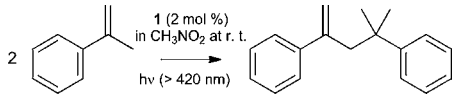

and bipyrimidine ligands can accelerate catalytic reactions.[8] The mononuclear complexes $[Ru(bpy)_2(bpm)]^{2+}$ and $[(bpy)PdMe(OCMe_2)]^+$ that are formally merged to constitute **1** were shown to be inactive toward AMS dimerization, both alone and as a 1:1 mixture.[7a]

Initially, the catalytic cycle sketched in Scheme 2 was proposed on the basis of experimental evidence. The initiation step should lead to the active hydrid compound **Int 1** by a first substitution of the acetone ligand by one α-methylstyrene molecule, followed by its insertion into the Pd–CH_3 bond to form the intermediate **2**, which undergoes subsequent β-H elimination to give **Int 1**. The catalytic mechanism is supposed to consist of successive migratory insertions (called insertion hereafter) of two substrate molecules. The first one should occur in the Pd–H bond (**Int 2**, see Scheme 2), which is stabilized by the coordination of a solvent molecule (L). The second insertion in the Pd–C bond results probably from the formation of complex **Int 3** by substitution of a solvent molecule by AMS. The resulting intermediate state (**Int 3**) gives rise to the AMS dimer, namely, 2,4-diphenyl-4-methyl-1-pentene, by β-H elimination. The rate-determining step is most probably the second insertion (step between **Int 3** and **Int 4**), which is assisted by visible light absorption (Scheme 2). Indeed, it was shown by NMR experiments coupled with the absence and the presence of light that light is necessary to activate the insertion process.[7] A thermal activation is possible (heating at 60 °C), but in that case, there is no selectivity. The advantage

Scheme 2. Proposed Catalytic Cycle for the Dimerization of AMS by 1

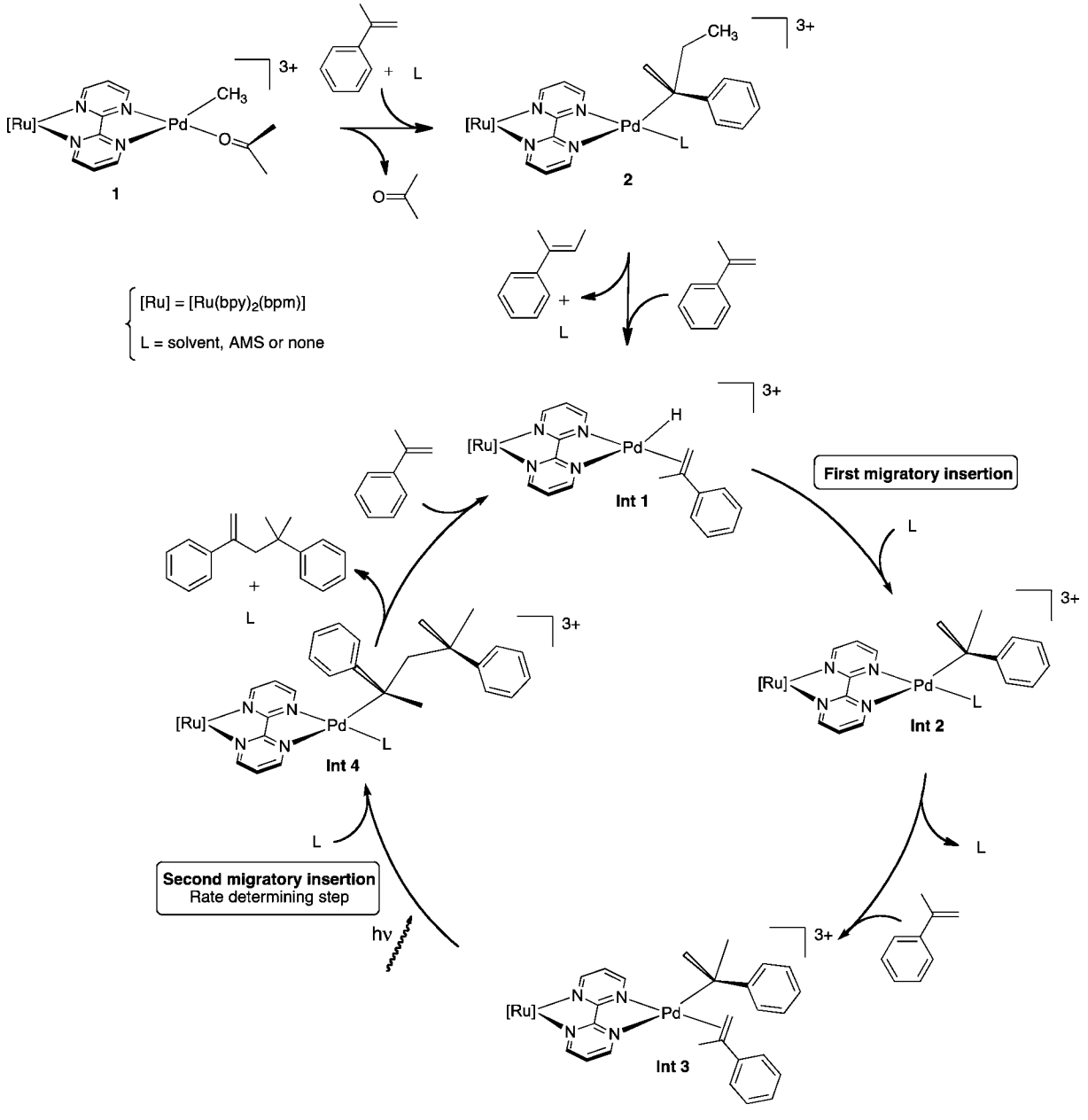

dx.doi.org/10.1021/ic400666v | Inorg. Chem. 2013, 52, 8030–8039

of photocatalytic reaction is not only a facile and low cost activation but also product selectivity. Indeed, complex **1** in the presence of AMS gives selectively 2,4-diphenyl-4-methyl-1-pentene upon light irradiation.

Nevertheless, the exact effect of light in the rate-determining step is still unclear. Since the key intermediates in the excited states are generated transiently, the means for their observation are limited. Therefore, it is worth investigating theoretically the photocatalytic reaction and, more specifically, the excited states of the intermediate complexes to elucidate how visible light activates the catalyst. The present theoretical study offers a panoramic view of this catalytic reaction to provide a fundamental understanding of this photocatalytic phenomenon, which could help in improving the catalytic system.

RESULTS AND DISCUSSION

The quality of the atomic basis set and the functional used in the following density functional theory (DFT) investigation were chosen on the basis of preliminary studies. The acetonitrile analogue of complex **1**, $[Ru(bpy)_2(bpm)PdMe(NCCH_3)]^{3+}$ $\mathbf{1}_{NCCH_3}$, was optimized (see the Appendix for computational details), and the pertinent structural parameters were compared to the X-ray data (Table S1, Supporting Information).[7a] On average, the discrepancy in the main distances between the two structures is 0.02 Å, with the more important deviation being 0.07 Å for the Pd−N(bpm) bond lengths. Angles are also well-reproduced (deviation < 2°). This agreement gives us confidence for the complexes discussed in the rest of the study for which no crystal structure is available.

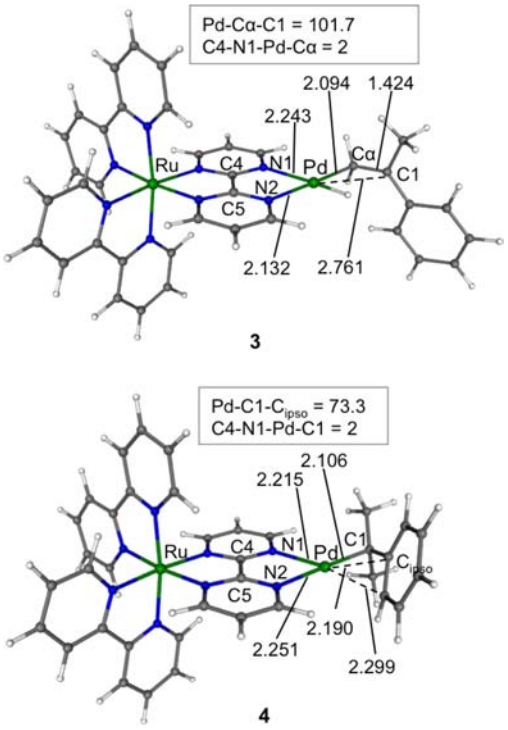

Figure 1. Optimized molecular structures of **3** and **4** (distances in Å, angles in deg).

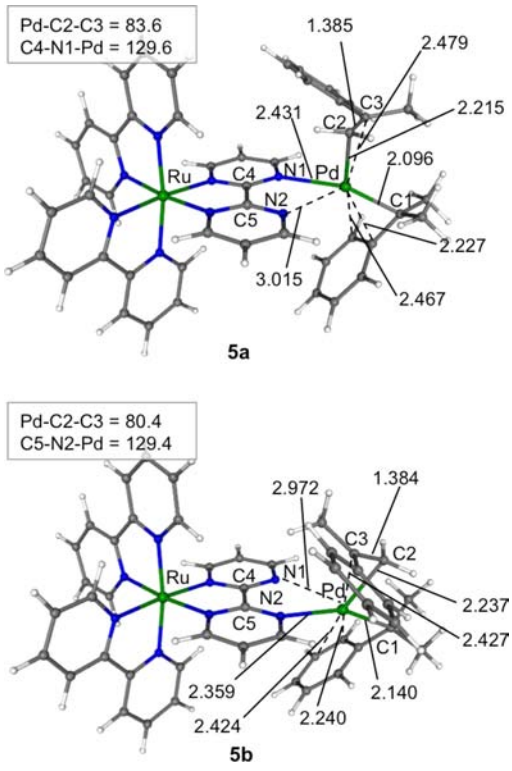

Figure 2. Optimized molecular structures of **5a** (top) and **5b** (bottom) (distances in Å, angles in deg).

First Coordination and Insertion of an AMS Molecule. Compound **1** is the precatalyst of the reaction (Scheme 2). The initiation step leads to compound **Int 1**, which is the real catalyst of dimerization of AMS. The geometry of **Int 1** was optimized and led to compound **3** (see Table S2, Supporting Information, and Figure 1). Its energy will be considered as the reference for the energy profile of the catalytic process. The palladium interaction with the C═C of AMS does not lead to a symmetric π-adduct as supposed in Scheme 2. As shown in Figure 1, the two Pd−C bond lengths strongly differ (2.094 and 2.761 Å). The most stable arrangement is characterized by a σ bond between Cα and Pd, and most probably an agostic bond between C1 and Pd. This description is supported by the fact

Scheme 3. Equilibrium Reaction of the Second Coordination of AMS ([Ru] = Ru(bpy)$_2$)

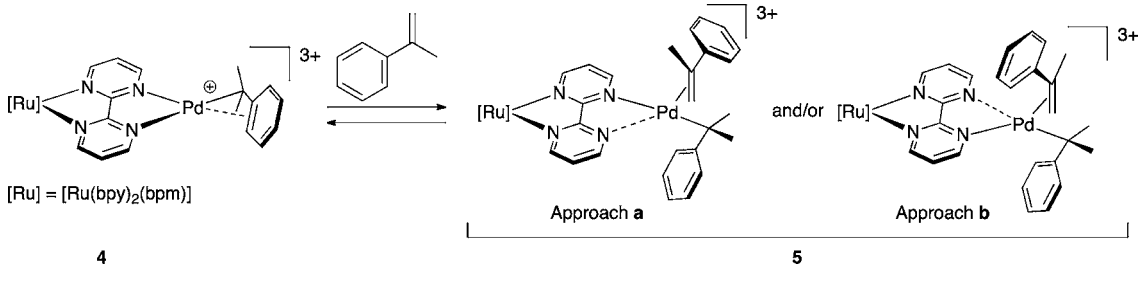

dx.doi.org/10.1021/ic400666v | Inorg. Chem. 2013, 52, 8030−8039

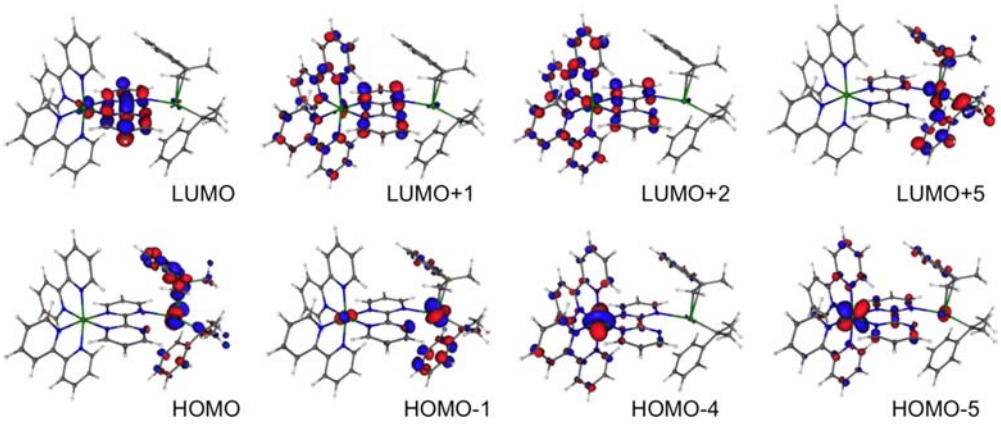

Figure 3. Selected frontier molecular orbitals of complex **5a**. Isocontour value ± 0.035 $(e{\cdot}bohr^{-3})^{1/2}$.

Table 1. Energy and Composition of the First Calculated Triplet Excited States (Transition Percentage ≥ 5%) of 5a and 5b

complex	state	E [eV]	E [10^4 cm^{-1}]	major contributions [%]
5a	T_1	2.13	1.72	94 HOMO (Pd/AMS) → LUMO (bpm)
	T_2	2.26	1.82	67 HOMO (Pd/AMS) → LUMO+5 (Pd/$CPhMe_2$)
				9 HOMO-6 (Pd/AMS/$CPhMe_2$) → LUMO+5 (Pd/$CPhMe_2$)
	T_3	2.26	1.82	65 HOMO-2 (Ru) → LUMO (bpm)
				10 HOMO-4 (Ru) → LUMO (bpm)
5b	T_1	1.95	1.58	95 HOMO (Pd/AMS) → LUMO (bpm)
	T_2	2.04	1.65	75 HOMO (Pd/AMS) → LUMO+5 (Pd/$CPhMe_2$)
	T_3	2.25	1.81	68 HOMO-3 (Ru) → LUMO (bpm)
				8 HOMO-1 (Pd/AMS) → LUMO (bpm)
				7 HOMO-4 (Ru/Pd) → LUMO (bpm)

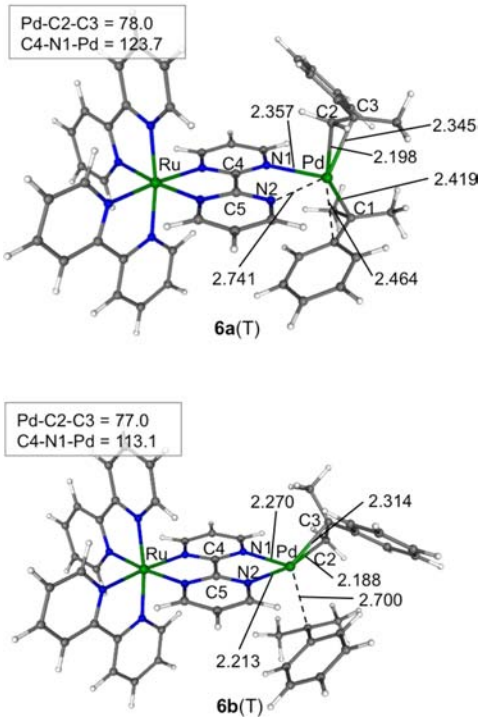

Figure 4. Optimized molecular structures of **6a**(T) (top) and **6b**(T) (bottom) (distances in Å, angles in deg).

that the carbon−carbon Cα−C1 distance of 1.424 Å is intermediate between a double bond and a single bond, and that the Pd−Cα−C1 angle is only 101.7°. This reinforced planar σ interaction is energetically favored over the perpendicular d−π interaction of the AMS π-adduct.

Taking into account the structural arrangement of **3**, the first insertion in the Pd−H bond of AMS, schematized as **Int 2** in Scheme 2, should be facilitated. Indeed, the resulting system **4** is calculated to be 79.3 $kJ{\cdot}mol^{-1}$ more stable than **3**. The energy barrier for this reaction through the transition state **TS1** was calculated to be 12.8 $kJ{\cdot}mol^{-1}$ (Cartesian coordinates of **TS1** given in Table S5, Supporting Information). An additional ligand L, as drawn in Scheme 2 for **Int 2**, was initially thought to be needed to complete the coordination sphere of the palladium(II) center to reach the 16-electron count usually observed for square planar complexes.[9] In fact, a M−CC agostic interaction occurs between one of the bonds of the phenyl group of the inserted AMS. Interestingly, such an arrangement is rarely observed.[10] As shown in Figure 1, the phenyl group of the inserted AMS is orientated in such a way that one of its C═C bonds, the one adjacent to the C_{ipso} carbon, interacts with the metal center. This C−C bond is consequently elongated (1.434 Å) and the Pd−C1−C_{ipso} angle is only 73.3°, revealing the geometrical constraint imposed by this bond.

Second AMS Coordination. The arrangement of **4** facilitates the approach of a substrate needed to obtain a compound of type **Int 3** (Scheme 2). Indeed, only a small internal reorganization (like a rotation along the Pd−C1 bond) is needed for a vacant site on the Pd center to be created. The resulting optimized structure **5** is shown in Scheme 3. For this system, different orientations of the approaching substrate can occur. We have considered several starting configurations, and two structures were finally found to be the more stable ones, namely, the conformers **5a** and **5b** of compound **5** issued from the approaches **a** and **b** shown in Scheme 3. Arrangement **a** is

dx.doi.org/10.1021/ic400666v | Inorg. Chem. 2013, 52, 8030−8039

Scheme 4. Equilibrium Reaction of the Second Coordination of AMS ([Ru] = Ru(bpy)$_2$)

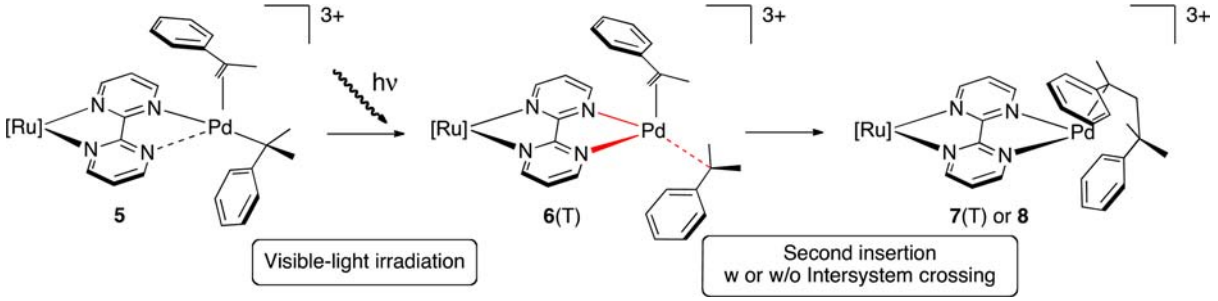

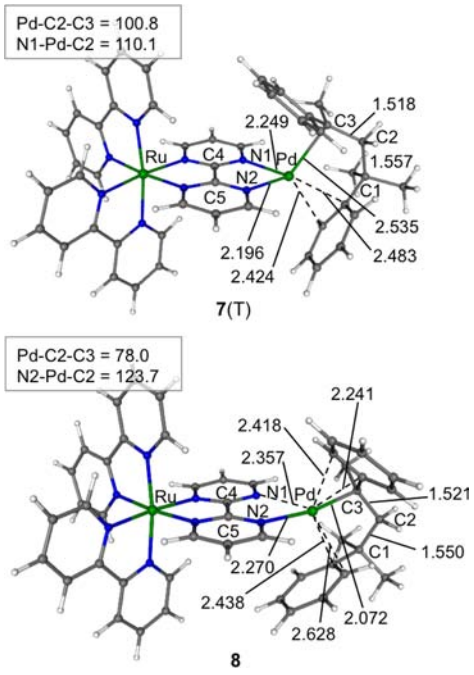

Figure 5. Optimized molecular structures of 7(T) (top) and **8** (bottom) (distances in Å, angles in deg).

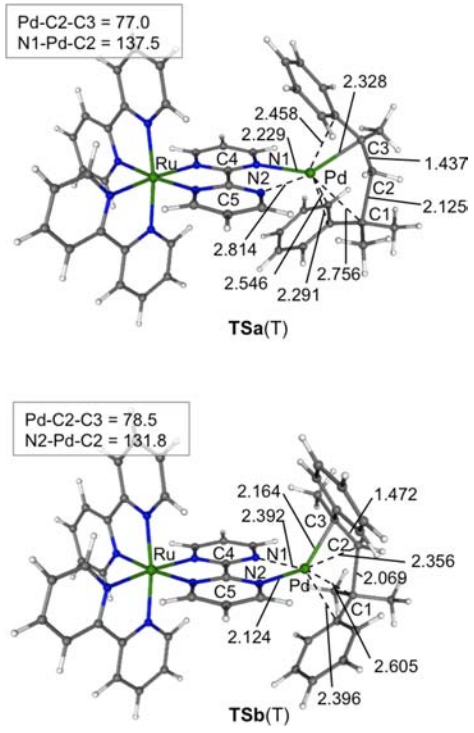

Figure 6. Optimized molecular structures of **TSa**(T) (top) and **TSb**(T) (bottom) (distances in Å, angles in deg).

12.8 kJ·mol^{-1} more stable than arrangement **b**. The geometry difference between the two conformers is the orientation of the phenyl of AMS, which is either on the side of the bpm ligand,

Scheme 5. Possible Paths of Reaction for the Second AMS Insertion after Visible Light Irradiation for Both Configurations a and b

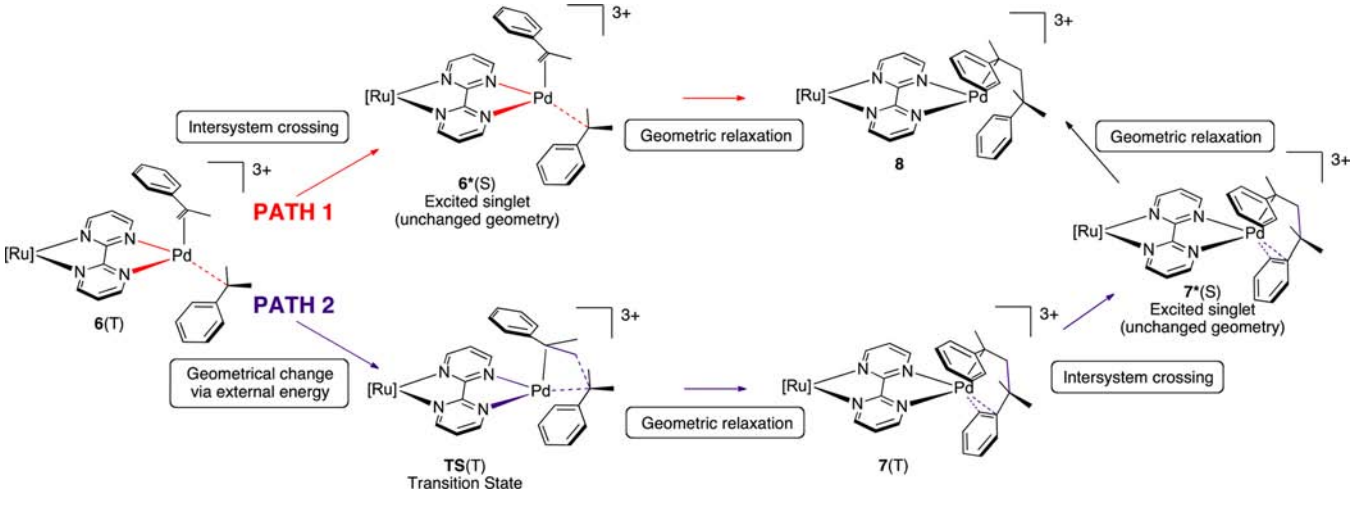

dx.doi.org/10.1021/ic400666v | Inorg. Chem. 2013, 52, 8030−8039

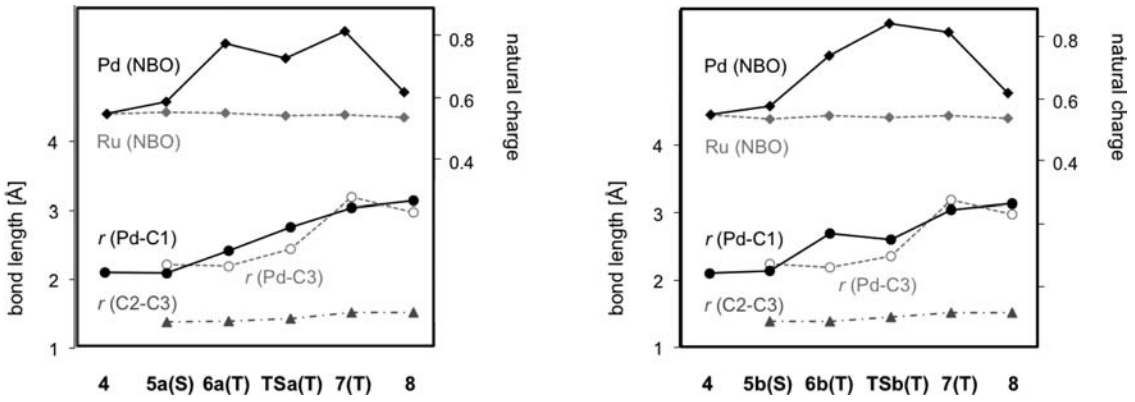

Figure 7. Changes of Pd−C1 and C2−C3 bond lengths and Pd and Ru NBO charges through the second insertion of AMS via **PATH 2** for the arrangements **a** (left) and **b** (right).

5a, or on the one of the inserted AMS, **5b**. The energy needed to coordinate the AMS is 14.6 kJ·mol^{-1} for **5a**, supporting the possibility to have an equilibrium between **4** and **5a** in solution at room temperature, as shown in Scheme 3 (the corresponding energy for **5b** is 27.1 kJ·mol^{-1}).

This second substrate coordination causes important structural changes around the Pd atom, the bpm becoming monodentate together with the formation of the AMS π-bonded adduct. The Pd(II) environment cannot be considered as square planar anymore (as postulated in Scheme 3), but closer to a 14-electron T-shaped one. Indeed, in **5a**, for example, the N2−Pd distance is considerably long (3.015 Å), whereas the Pd−N1 bond is much shorter (2.431 Å) (see Figure 2). The M−CC agostic bond present in arrangement **4** is not present anymore after the second AMS addition. The palladium−carbon bonds can be described as intermediate between a simple Pd−alkyl bond and a π−allyl−palladium contact for the added AMS, and as that of π−alkene−palladium type for the inserted one.

The calculated electronic structure of **5a** presents a significant energy gap between occupied and virtual molecular orbitals (MOs) (2.92 eV at LANL2DZP/mPW1PW91). Selected MOs of the HOMO−LUMO region are shown in Figure 3. The HOMO and HOMO-1 have a predominant coordinated-AMS character associated with a smaller Pd character (roughly 60% and 30%, respectively). On the contrary, the HOMO-2, HOMO-4, and HOMO-5 are mainly ruthenium centered. The HOMO-3 is mostly ligand in character (78%) and can be described as a π orbital of the phenyl of the coordinated AMS (12% Ru). The five first LUMOs are π*-type orbitals, located on either the bpm or the bpy π-acceptor ligands. For instance, the LUMO is mainly bpm in character (72%). On the other hand, the LUMO+5 is localized on the Pd atom and on the inserted AMS (25% and 58%, respectively).

Photoactivation at the Molecular Level. At this stage, it has been shown experimentally that the solution needs to be irradiated in the visible region in order to induce catalytic reaction (**Int 3** to **Int 4** in Scheme 2).[7a] Indeed, when AMS is added to a solution of **1**, first insertion of AMS, followed by the formation of intermediate **5**, was proved experimentally. Experimental results indeed reveal its formation, and no further product was observed under the dark condition upon addition of AMS. Light irradiation to the mixture of **5** and AMS resulted in the catalytic formation of an AMS dimer.[7a] To support these experimental findings, the activation energies were calculated via the optimization of the possible transition states (in singlet state configuration), which led to the second insertion. The high calculated energy barriers, 111 kJ·mol^{-1} starting from **5a** and 84.7 kJ·mol^{-1} starting from **5b** (coordinates of the transition states **TSa**(S) and **TSb**(S) given in the Supporting Information), allow us to conclude that insertion cannot proceed at room temperature. We consider that the advantage of the photocatalytic reaction is not only the low-energy cost but also the product selectivity. In our case, complex **1** gave 2,4-diphenyl-4-methyl-1-pentene selectively from AMS addition upon light irradiation, whereas complex **1**, heated at 60 °C, without irradiation, yielded several different isomeric AMS oligomers. Although the way of activation is essentially different from the irradiation condition, the difference in the reaction product between the two conditions is mainly attributed to the selective activation of molecules within a narrowly distributed energy range. Whereas light irradiation activates only the part of the molecules that absorbs at specific wavelengths, heating impacts the whole reaction mixture. The latter involves a transfer of excess energy, which will cause side reactions.

Obviously, the reaction needs to be photocatalytically facilitated as experimentally demonstrated.[7] These results indicate that photoexcitation of **5** is essential for the second insertion of AMS. We need then to investigate the consequences of exciting complex **5**.

Therefore, time-dependent DFT (TD-DFT) calculations were first performed to study the vertical excitations of **5**. The lower singlet and triplet excited states were considered (see Table S3, Supporting Information, and Table 1, respectively). The excited states (S_n) having a significant oscillator strength should be the ones with the highest probability of absorbing light experimentally. Three excited singlets, which fulfill this statement, were identified. They all correspond to a charge transfer from one of the metal−ligand moieties to the bpm ligand. The most intense absorption is predicted to be at 2.80 eV for **5a**, for example. The excitation corresponds predominantly from the Ru atom to the bpm ligand and is described principally by a transition from the HOMO-5 to the LUMO (see Figure 3). This is in agreement with the general assumption that the $[Ru(bpy)_3]^{2+}$ derivatives are good visible light absorbers.

Experimentally, a fast and highly efficient ($\eta_{ISC} \sim 1$) intersystem crossing (ISC) was revealed by ultrafast spectroscopic techniques after irradiation of **5**.[7] The generated triplet excited state is relatively long-lived ($\tau \sim 90$ ns for **1**), which allows a geometric relaxation process to occur. Indeed, the

dx.doi.org/10.1021/ic400666v | Inorg. Chem. 2013, 52, 8030−8039

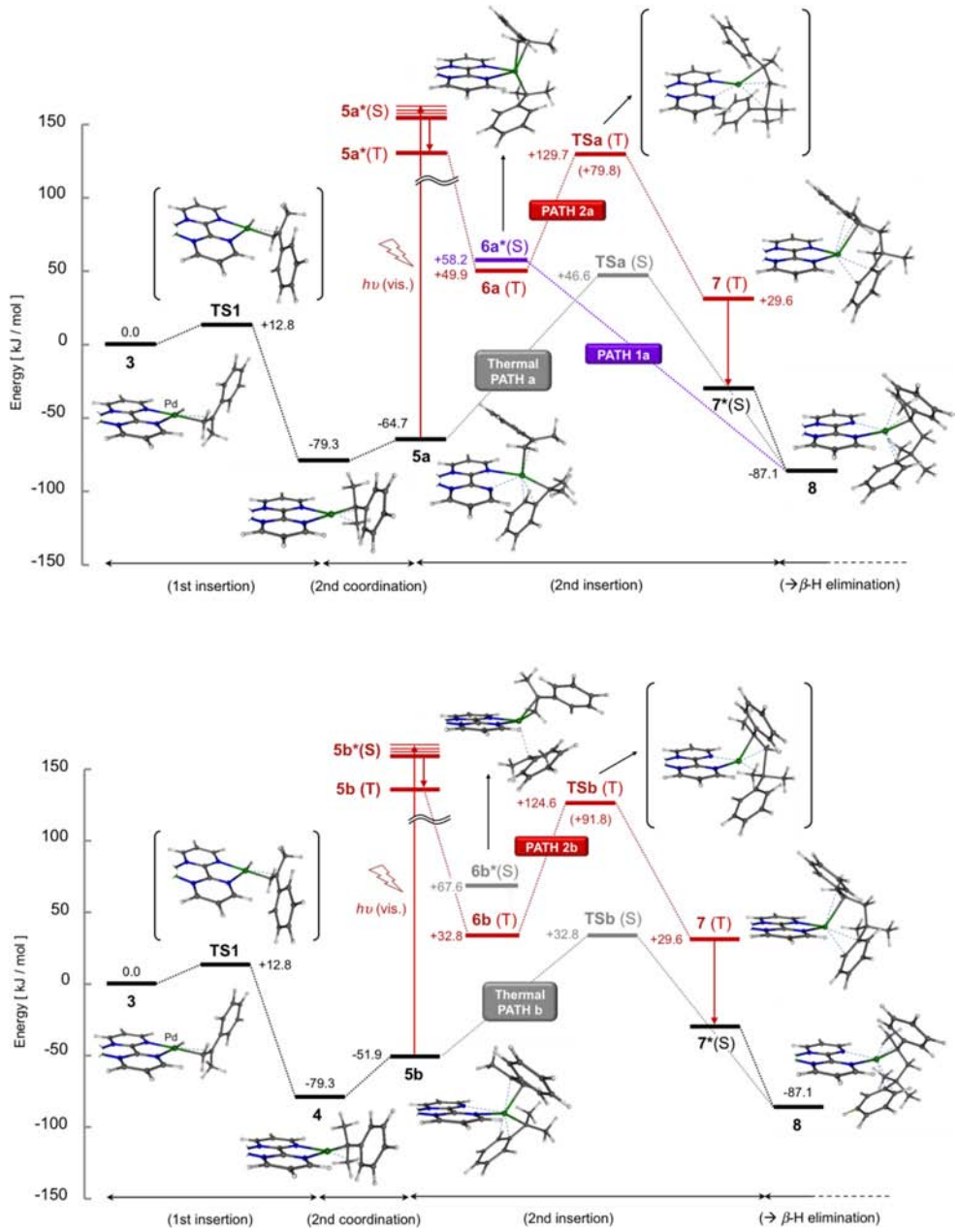

Figure 8. Gibbs free energy profile (ΔG_v^0) at 298 K and optimized structures of the intermediates, transition states, and excited states involved in the thermal path (**Thermal PATH**) and photoexcited-activated (**PATH 1** and **PATH 2**) second coordination and insertion of AMS, for arrangement **a** (top), and arrangement **b** (bottom) (see Table S6, Supporting Information, for energy values). The Ru−polypyridyl moiety is omitted for the sake of clarity.

reaction rate is considerably lower by addition of O_2, revealing the presence of triplet species that are crucial for the reaction. In accordance with the Kasha's rule, the lowest triplet excited state T_1 is probably populated. Indeed, we tried several geometry optimizations for other low-lying triplet states (T_n, $n > 2$) using the TD-DFT method. No noticeable geometrical changes were observed around the Pd unit, contrary to the relaxation of the T_1 state (see below). Geometrical reorganization is necessary for the second insertion to occur.

The geometries of the first triplet excited state of **5a** and **5b** were optimized (see Table S2, Supporting Information), leading to two new stable arrangements **6a**(T) and **6b**(T). The main structural modification between **5** and **6**(T) is the stronger and more symmetrical bonding between the nitrogen atoms of the bpm central ligand and the Pd atom. This is accompanied by a marked elongation of the Pd−C1 bond (0.323 and 0.560 Å for **6a** and **6b**, respectively).

Clearly, the initial metal/ligand charge-transfer phenomenon to the bpm ligand is followed by a modification of its bonding contacts with the Pd center after geometrical relaxation (Figure 4). This geometrical relaxation can be understood from the TD-DFT results. Indeed, the first triplet excitation of **5** corresponds formally to an electron transfer from the HOMO (Pd/AMS) to the LUMO (π^* bpm), leading to a decrease of electron density on the Pd part in favor of the bpm ligand. The geometrical relaxation induced by this electron transfer will clearly partly compensate this loss by a Pd−N1 shortening.

dx.doi.org/10.1021/ic400666v | Inorg. Chem. 2013, 52, 8030−8039

This probably favors a slight Pd−C1 elongation since the C1 atom is somewhat in a *trans* position of the N1 atom.

Natural bond orbital (NBO) analyses were performed for **5** and **6**(T). The results, detailed in the Supporting Information, indicate that the natural charge on Pd remarkably increases after irradiation (from +0.593 to +0.783 for **5a** to **6a**(T), respectively, and from +0.584 to +0.747 for **5b** to **6b**(T), respectively), whereas the charge on Ru hardly changes. Thus, the palladium center becomes electron poorer upon excitation.

Second Insertion of AMS. The long Pd−C1 distance found in **6**(T) is favorable to the occurrence of the substrate insertion. To further explore this reaction process, the possible evolutions of **6**(T) to transition states or to the intersystem crossing process have to be diagnosed. To obtain data on the possible de-excitation/insertion scheme, the arrangement of the inserted-AMS compounds is necessary. We thus optimized the possible insertion products, which can be either triplet **7**(T) or singlet **8** (Scheme 4). Several starting configurations were considered (different orientations of the AMS dimer with respect to the bpm unit). The most stable arrangements are shown in Figure 5. They both display a nonconventional arrangement of the coordination sphere of the Pd center. **7**(T) is 1.33 eV higher in energy than **8**, but its participation in the catalytic cycle cannot be excluded without the calculation of the energetic barrier that can be found along the reaction.

For **8**, the fact that the Pd and C1 atoms are separated by 3.135 Å, associated with the short C1−C2 distance (1.550 Å), allows us to consider the second AMS as inserted. An asymmetrical coordination of the bpm ligand is found (N1−Pd = 2.627 Å, Pd−N2 = 2.270 Å). This type of arrangement was already observed for **5**. The loss of electrons is compensated by π interactions between the Pd center and the two phenyl rings of the inserted styrene to reach the 16-electron count.

For **7**(T), the second AMS is also undoubtedly inserted. The bpm−Pd bonding is symmetric, contrary to **8**; thus, only one phenyl π interaction is needed to stabilize the Pd center. As illustrated in Scheme 5, two possible processes can occur from the triplet state **6**(T) of configuration **a** or **b**: (i) either an ISC to lead to a singlet spin-state excited species (**6***(S)), which will give **8** (**PATH 1**), (ii) or an activated geometric evolution via a triplet transition state (**TS**(T)) to give **7**(T), followed by an ISC (**7***(S)) and a relaxation to give compound **8** (**PATH 2**). We have thus investigated the possible transition states (starting from **6a**(T) and **6b**(T) arrangements) present in the second insertion process and evaluated their probability of undergoing ISC taking into account spin−orbit coupling (see the Appendix).

The transition states **TSa**(T) and **TSb**(T) were calculated starting from **6a**(T) and **6b**(T), respectively. Their main geometrical data are given in Figure 6. Whereas the Pd center is kept at a relatively short distance from C3 (2.328 Å for **TSa**(T), 2.164 Å for **TSb**(T)), the Pd−C2 distance is much longer for the transition states than for the activated species **6**(T). Meanwhile, the average C2−C3 distance is somewhat elongated from 1.393 Å to 1.454 Å, intermediate between a double bond and a single bond. The Pd−C1 contact is weakened (2.756 Å for **TSa**(T), 2.605 Å for **TSb**(T)). This weakening is counterbalanced by a stabilizing interaction between Pd interaction and the *ipso*-carbon atom linked to C1 (2.291 Å for **TSa**(T), 2.396 Å for **TSb**(T)). Furthermore, the Pd−N bond in the *trans* position to C1−C_{ipso} is reinforced in the transition state. These interactions contribute to stabilize the Pd center during the insertion process. All of these geometrical features reflect the evolution of these transition states toward the second AMS insertion in which the C1−C2 bond will be formed.

The evolution of the most important bond lengths and natural charges on the metal centers throughout the reaction **PATH 2** is summarized in Figure 7 for both arrangements **a** and **b**. In each case, the NBO charge of the Pd center slightly increases until reaching the transition state (ca. +0.2 higher than that of the ground state) and next decreases back to its initial value after insertion. Interestingly, the NBO charge of the Ru center is hardly modified. This is in agreement with the geometry analysis that revealed that the weakening of Pd−N or Pd−C bonds is always associated with strengthening of others. This supports also the fact that no additional ligand is needed to compensate for the loss of electrons around Pd during the process, the flexibility of the bpm ligand and presence of phenyl groups being sufficient for an internal stabilization.

The study of the Pd−C1 and Pd−C2 distances indicates that their increase is regular along **PATH 2** to reach the intermediate **8** in which the second AMS is inserted. The C2−C3 bond is slightly elongated (by 0.14 Å), leading to a diminishing of its bond order, becoming close to a single bond. The analysis of the calculated imaginary vibrational frequency shows unambiguously that the reaction coordinate is mainly the shortening of C1−C2. The corresponding Gibbs free energy barrier for this AMS insertion going from **6**(T) to **7**(T), **PATH 2**, is 79.8 kJ·mol^{-1} starting from arrangement **a**, and 91.8 kJ·mol^{-1} from **b**.

As shown in Scheme 5, ISC can occur at different steps of the reaction process. For **PATH 1**, it should occur after the geometric relaxation of the triplet excited state that leads to **6**(T). This ISC was evaluated by spin−orbit-coupling calculations with the geometry of **6**(T) (see the Appendix). The lifetime of **6**(T) is expected to be 1.8 ms (based on the oscillator strength value) before ISC. The resulting excited singlet state **6***(S) is almost isoenergetic (+1.7 kJ·mol^{-1}) to **6**(T) for arrangement **a**, whereas it is much higher in energy (+34.8 kJ·mol^{-1}) for **b**, discarding this latter possibility. The geometric relaxation of the **6a***(S) excited state leads directly to **8**. The search of possible transition states or intermediates shows that the relaxation proceeds directly without additional energy (Figure 8).

Evaluation of the Lowest-Energy Reaction Path. The calculated energy profiles summarizing the whole results detailed above are given in Figure 8, for the substrate approaches **a** (top) and **b** (bottom). Clearly, as mentioned above and in agreement with the experimental results, the energy barriers of 111.3 and 84.7 kJ·mol^{-1} for the thermal paths **a** and **b** prevent the second insertion reaction to occur at room temperature. This is in agreement with the experimental results. Indeed, it was shown experimentally that the solution has to be heated to 60 °C to induce a reaction that is nonselective.

The photocatalysis, which was shown to be selective and efficient, can proceed in different steps, that is, intersystem crossings and geometry relaxations, involving or not an energy barrier that can occur in a different order. Two paths were revealed by DFT calculations for approaches **a** and **b**, as summarized in Figure 8. In both cases, the initialization leads to a hydrido−AMS complex **3** (see Scheme 2, **Int 1**) and is followed by the first AMS insertion into the Pd−H bond to lead to complex **4**. Interestingly, complex **4** does not necessitate an additional ligand to be stable, as supposed in Scheme 2 (**Int**

dx.doi.org/10.1021/ic400666v | *Inorg. Chem.* 2013, 52, 8030−8039

2), but the presence of an agostic interaction between the two carbon atoms of the phenyl group of the inserted AMS is enough to stabilize the system.[10] The approach of the second AMS can be done oppositely to the first inserted AMS (approach **a**), leading to arrangement **5a**, or side-on (approach **b**), giving arrangement **5b**. The former is slightly more stable (+12.9 kJ·mol^{-1}) than the latter, but this energy difference does not allow excluding the possibility of having **5b** in solution. It was shown that light excitation is needed at this stage of the reaction since no evolution is observed in the absence of light at that step of the reaction. Quantum chemical calculations of the excitation and relaxation of **5** allow providing two conformers of the triplet intermediate **6**(T).

A first possibility, **PATH 2** (see Figure 8), is that this triplet intermediate evolves to the inserted AMS structure **7**(T) via a transition state that was calculated to be more than 80 kJ·mol^{-1} higher in energy in both cases. Even though light irradiation could have locally heated the solution (nonradiative de-excitations), this energy barrier is too important to be overcome.

A second possibility **PATH 1** (see Figure 8) consists in having an ISC immediatly after the geometry relaxation. Calculations indicated that it was not possible for the arrangements **b**. On the contrary, it is highly probable for **6a**(T). In that case, once the molecule becomes a singlet, it relaxes without any transition state or intermediate into **8**. β-H elimination of the AMS dimer is thus straightforward together with the coordination of the new AMS molecule. Compound **3** is thus reformed and available for a new catalytic cycle.

CONCLUSION

Reaction and photochemical processes for the second insertion step of the photocatalytic dimerization of AMS by a Ru−Pd dinuclear complex were investigated by quantum chemical (DFT and TD-DFT) calculations. Our results show that the initiation stage concerns the Ru−polypyridyl unit, which contributes to the photoexcitation process by involving efficient absorption of visible light. It can stabilize the low-lying unoccupied molecular orbitals based on the bridging bipyrimidine ligand and lower the excitation energies. The ruthenium moiety can be seen as a photocatalytic antenna. For future investigations, modifications of its surrounding ligands should be driven toward higher efficiency of absorption without inducing electronic modifications of the Pd moiety. Indeed, the catalytic reaction is localized only on the Pd moiety once it is photoactivated.

The presence of phenyl groups in the AMS substrate allows a compensation of the loss of electron density on the Pd center along the catalytic reaction. For example, it is the case during the first AMS insertion in the Pd−H bond of the complex, or when a geometric reorganization is induced by visible light absorption. Irrespective of the targeted catalytic organic synthesis, the presence of carbon−carbon double bonds (phenyl groups here) in the substrate is mandatory. The bpm ligand was also shown to be versatile, according to our theoretical study, being able to mono- or bicoordinate the Pd atom. Any change or substitution of the bpm ligand should be done in order to keep this ability. Interestingly, this fact implies that no additional molecule, substrate, or solvent is needed for the reaction to proceed. Finally, we have shown that light irradiation opens up a favorable pathway that has no energy barrier. Overall, the selectivity, the efficiency, and the sustainability of the AMS photocatalytic coupling are remarkable, since, taken all together, the reaction is atom-saving (no additional molecule needed) and fast (since no molecule diffusion is needed). It needs a costless energy (since visible light is an unlimited energy source), and is selective (only one efficient reaction path). Following this study, we are currently carrying out new experiments tailoring the catalyst to, first, improve the reaction and, second, to render it active for other organic syntheses.

APPENDIX

Calculations were performed at the DFT level with the Gaussian 09 package.[11] The geometry optimizations were performed using the mPW1PW91 functional.[12] The LanL2DZ basis set was used for all atoms and extended by a polarization function (except for H).[13] To address solvation effects, the polarizable continuum model (PCM)[14] was used for the ground and excited states. Attempts to enlarge the basis set were unsuccessful (SCF divergence for LanL2TZ(f)). For validation, vibrational frequencies were calculated for all ground states, intermediates, and transition states. B3PW91 single-point calculations were performed to test the robustness of the results toward the functionals (see the Supporting Information). The orbital plots as well as the graphical representations were performed using Molekel.[15] Natural bond orbital (NBO) analysis was used to predict and interpret the computational results.[16] SWizard was used to simulate the absorption spectra.[17] Total ZPE energies and Cartesian coordinates of computed structures are given in Table S5 (Supporting Information).[18] DFT two-component spin−orbit coupling calculations were performed with the ADF2012.01 package.[19] For these calculations, the nonlocal corrections of Adamo−Barone and of Perdew−Burke−Ernzerhof (*m*PBE) were added to the exchange and correlation energies, respectively.[20] Tamm−Dancoff approximation calculations were used to evaluate the lifetime of the excited states and the oscillator strength.[21]

ASSOCIATED CONTENT

Supporting Information

Selected geometric experimental and theoretical data of $\mathbf{1}_{NCCH_3}$; selected geometric theoretical data for **3**, **4**, **5a**, **5b**, **6a**(T), **6b**(T), **TSa**(T), **TSb**(T), **7**(T), and **8**; TD-DFT calculations for **5a** and **5b**; NBO calculations for **5a**, **5b**, **6a**(T), and **6b**(T); Cartesian coordinates and energies of all optimized structures; and corrected Gibbs free and ZPE energies. This material is available free of charge via the Internet at http://pubs.acs.org.

AUTHOR INFORMATION

Corresponding Author

*E-mail: jean-francois.halet@univ-rennes1.fr (J.-F.H.), karine.costuas@univ-rennes1.fr (K.C.).

Present Address

[‖]Precursory Research for Embryonic Science and Technology, Japan Science and Technology Agency (JST-PRESTO), 4-1-8 Honcho, Kawaguchi, Saitama 332-0012, Japan.

Notes

The authors declare no competing financial interest.

ACKNOWLEDGMENTS

K.M. thanks the Collège Doctoral Franco-Japonais (CDFJ) and the International Doctoral College of the European University of Brittany (CDI - UEB), France, for her visit to Rennes. This

research was also financially supported by the Japan Science and Technology Agency, PRESTO (Precursory Research for Embryonic Science and Technology; A.I.), a Grant-in-Aid for JSPS Fellows (K.M.), the Naito Foundation (A.I.), and the Hayashi Memorial Foundation for Female Natural Scientists (K.M.). Computations were performed using HPC resources from GENCI-CINES and GENCI-IDRIS (Grants 2012-80649, 2013-80649), which are gratefully acknowledged.

REFERENCES

(1) Vos, J. G.; Pryce, M. T. *Coord. Chem. Rev.* **2010**, *254*, 2519.
(2) See, for examples: (a) Juris, A.; Balzani, V.; Barigelletti, F.; Campagna, S.; Belser, P.; Von Zelewsky, A. *Coord. Chem. Rev.* **1988**, *84*, 85. (b) Vos, J. G.; Kelly, J. M. *Dalton Trans.* **2006**, 4869. (c) Campagna, S.; Puntorliero, F.; Nastasi, F.; Bergamini, G.; Balzani, V. *Top. Curr. Chem.* **2007**, *280*, 117. (d) Inagaki, A.; Akita, M. *Coord. Chem. Rev.* **2010**, *254*, 1220.
(3) (a) Rau, S.; Schafer, B.; Gleich, D.; Andres, E.; Rudolph, M.; Freidrich, M.; Gorls, H.; Henry, W.; Vos, J. G. *Angew. Chem., Int. Ed.* **2006**, *45*, 6215. (b) Ozawa, H.; Yokoyama, Y.; Haga, M.; Sakai, K. *Dalton Trans.* **2007**, 1197. (c) Fihri, A.; Arteno, V.; Pereira, A.; Fontecave, M. *Dalton Trans.* **2008**, 5567. (d) Tschierlei, S.; Presselt, M.; Kuhnt, C.; Yartsev, A.; Pascher, T.; Sundström, V.; Karnahl, M.; Schwalbe, M.; Schäfer, B.; Rau, S.; Schmitt, M.; Dietzek, B.; Popp, J. *Chem.—Eur. J.* **2009**, *15*, 7678. (e) Ozawa, H.; Sakai, K. *Chem. Commun.* **2011**, *47*, 2227.
(4) Takeda, H.; Ishitani, O. *Coord. Chem. Rev.* **2010**, *254*, 346.
(5) (a) Ozawa, H.; Haga, M.; Sakai, K. *J. Am. Chem. Soc.* **2006**, *128*, 4926. (b) Ozawa, H.; Kobayashi, M.; Balan, B.; Masaoka, S.; Sakai, K. *Chem.—Asian J.* **2010**, *5*, 1860. (c) Ajayakumar, G.; Kobayashi, M.; Masaoka, S.; Sakai, K. *Dalton Trans.* **2011**, *40*, 3955.
(6) (a) Gholamkhass, B.; Mametsuka, H.; Koike, K.; Tanabe, T.; Furue, M.; Ishitani, O. *Inorg. Chem.* **2005**, *44*, 2326. (b) Bian, Z.; Sumi, K.; Furue, M.; Sato, S.; Koike, K.; Ishitani, O. *Inorg. Chem.* **2008**, *47*, 10801. (c) Tamaki, Y.; Watanabe, K.; Koike, K.; Inoue, H.; Morimoto, T.; Ishitani, O. *Faraday Discuss.* **2012**, *155*, 115.
(7) (a) Inagaki, A.; Edure, S.; Yatsuda, S.; Akita, M. *Chem. Commun.* **2005**, 5468. (b) Inagaki, A.; Yatsuda, S.; Edure, S.; Suzuki, A.; Takahashi, T.; Akita, M. *Inorg. Chem.* **2007**, *46*, 2432.
(8) Nitadori, H.; Takahashi, T.; Inagaki, A.; Akita, M. *Inorg. Chem.* **2011**, *51*, 51.
(9) Albright, T. A.; Burdett, J. K.; Whangbo, M.-H. *Orbital Interactions in Chemistry*; John Wiley & Sons: New York, 1985.
(10) See, for recent examples: (a) Stępień, M.; Latos-Grażyński, L.; Szterenberg, L.; Panek, J.; Latajka, Z. *J. Am. Chem. Soc.* **2004**, *126*, 4566. (b) Chang, G.-F.; Wang, C.-H.; Lu, H.-C.; Kan, L.-S; Chao, I.; Chen, W. H.; Kumar, A.; Lo, L.; dela Rosa, M. A. C.; Hung, C.-H. *Chem.—Eur. J.* **2011**, *17*, 11332.
(11) Frisch, M. J.; Trucks, G. W.; Schlegel, H. B.; Scuseria, G. E.; Robb, M. A.; Cheeseman, J. R.; Scalmani, G.; Barone, V.; Mennucci, B.; Petersson, G. A.; Nakatsuji, H.; Caricato, M.; Li, X.; Hratchian, H. P.; Izmaylov, A. F.; Bloino, J.; Zheng, G.; Sonnenberg, J. L.; Hada, M.; Ehara, M.; Toyota, K.; Fukuda, R.; Hasegawa, J.; Ishida, M.; Nakajima, T.; Honda, Y.; Kitao, O.; Nakai, H.; Vreven, T.; Montgomery, J. A., Jr.; Peralta, J. E.; Ogliaro, F.; Bearpark, M.; Heyd, J. J.; Brothers, E.; Kudin, K. N.; Staroverov, V. N.; Kobayashi, R.; Normand, J.; Raghavachari, K.; Rendell, A.; Burant, J. C.; Iyengar, S. S.; Tomasi, J.; Cossi, M.; Rega, N.; Millam, J. M.; Klene, M.; Knox, J. E.; Cross, J. B.; Bakken, V.; Adamo, C.; Jaramillo, J.; Gomperts, R.; Stratmann, R. E.; Yazyev, O.; Austin, A. J.; Cammi, R.; Pomelli, C.; Ochterski, J. W.; Martin, R. L.; Morokuma, K.; Zakrzewski, V. G.; Voth, G. A.; Salvador, P.; Dannenberg, J. J.; Dapprich, S.; Daniels, A. D.; Farkas, Ö.; Foresman, J. B.; Ortiz, J. V.; Cioslowski, J.; Fox, D. J. *Gaussian 09*, Revision A.2; Gaussian, Inc.: Wallingford, CT, 2009.
(12) Adamo, C.; Barone, V. *J. Chem. Phys.* **1998**, *108*, 664.
(13) (a) Dunning, T. H.; Hay, P. J. In *Modern Theoretical Chemistry*; Schaefer, H. F., III, Ed.; Plenum: New York, 1976; Vol. 3, p 1. (b) Wadt, W. R.; Hay, P. J. *J. Chem. Phys.* **1985**, *82*, 284. (c) Wadt, W. R.; Hay, P. J. *J. Chem. Phys.* **1985**, *82*, 299.
(14) Tomasi, J.; Mennucci, B.; Cammi, R. *Chem. Rev.* **2005**, *105*, 2999.
(15) Varetto, U. *Molekel 5.4*; Swiss National Supercomputing Centre: Lugano, Switzerland, 2009.
(16) Glendening, E. D.; Badenhoop, J. K.; Reed, A. E.; Carpenter, J. E.; Bohmann, J. A.; Morales, C. M.; Weinhold, F. *NBO 5.0*; Theoretical Chemistry Institute, University of Wisconsin: Madison, WI, 2001.
(17) (a) Gorelsky, S. I. *SWizard Program*; University of Ottawa: Ottawa, Canada, 2012. http://www.sg-chem.net/. (b) Gorelsky, S. I.; Lever, A. B. P. *J. Organomet. Chem.* **2001**, *635*, 187.
(18) Scalmani, G.; Frisch, M. J.; Mennucci, B.; Tomasi, J.; Cammi, R.; Barone, V. *J. Chem. Phys.* **2006**, *124*, 094107.
(19) (a) te Velde, G.; Bickelhaupt, F. M.; Baerends, E. J.; Fonseca Guerra, C.; van Gisbergen, S. J. A.; Snijders, J. G.; Ziegler, T. *J. Comput. Chem.* **2001**, *22*, 931. (b) *ADF2012.01*; SCM, Theoretical Chemistry, Vrije Universiteit: Amsterdam, The Netherlands. www.scm.com.
(20) (a) Adamo, C.; Barone, V. *J. Chem. Phys.* **2002**, *116*, 5933. (b) Perdew, J. P.; Burke, K.; Ernzerhof, M. *Phys. Rev. Lett.* **1996**, *77*, 3865.
(21) Hirata, S.; Head-Gordon, M. *Chem. Phys. Lett.* **1999**, *314*, 291.